International Journal of Civil Engineering

Geotechnical Engineering

Seismic behavior of topographic features with material damping using BEM in time domain

M. Afzalirad[1], M. Kamalian[2,*], M.K. Jafari[3], A. Sohrabi-Bidar[4]

Received: January 2012, Revised: September 2012, Accepted: November 2012

Abstract

In this paper, an advanced formulation of time-domain, two-dimensional Boundary Element Method (BEM) with material damping is presented. Full space two-dimensional visco-elastodynamic time-convoluted kernels are proposed in order to incorporate proportional damping. This approach is applied to carry out site response analysis of viscoelastic topographic structures subjected to SV and P incident waves. Seismic responses of horizontally layered site, semi-circular canyons, slope topography and ridge sections subjected to these incident waves are analyzed in order to demonstrate the accuracy of the kernels and the applicability of the presented viscoelastic boundary element algorithm. The results show an excellent agreement with recent published results obtained in frequency domain. Also, the effects of different material damping ratios on site response are investigated.

Keywords: *BEM; Visco-elastodynamic kernels, Time domain, Viscoelastic, Topography effects.*

1. Introduction

It is well established that the seismic ground response of surface topographies may differ from those of free-field motion during earthquakes. Although the topography effect on ground response could be very important when the wavelength is comparable to irregularity dimensions [1], there are only few building codes, which have considered this issue. This is because of the complex nature of seismic wave scattering by topographical structures, which can only be solved accurately and economically using advanced numerical methods under realistic conditions.

The boundary element method (BEM) is a very effective numerical tool for dynamic analysis of linear elastic bounded and unbounded media. The main advantage of this method is that the discretization is done only on the boundary, yielding smaller meshes and systems of equations.

Another advantage is that this method automatically satisfies Sommerfeld's radiation conditions at infinity and there is no need to model the far field in problems with semi-infinite or infinite domains. It is clear that time-domain boundary element in comparison with frequency domain can extend to the nonlinear behavior and also, it can be combined with finite element method (FEM).

Regarding the application of BEM for site response analyses of topographic structures in the time domain, Antes and Von-Estorff (1988) [2] were the first who studied the seismic response amplification from topography using a two-dimensional hybrid boundary element/finite element method. Takemiya and Fujiwara (1994) [3] used a time-domain 2D BEM to analyze the seismic response of canyons and alluvial basins, but their formulation was restricted to the scattering of anti-plane (SH) waves, which involves less computational effort. Adam and Takemiya (1996) [4] and Takemiya and Adam (1997, 1998) [5, 6] studied the seismic wave amplification from 2D topography and geological conditions in the Kobe valley during the Hyogo-Ken Nanbu earthquake using a hybrid boundary element/finite element method. Recently Kamalian et al. (2003, 2006) [7, 8] applied the time domain boundary element method and the hybrid time domain boundary element/finite element method to analyze the scattering and diffraction of P and SV waves by homogenous and non-homogenous topographic structures. In their research, Kamalian et al. (2007, 2008a, b) [9- 11] used a direct boundary element method to study the amplification pattern of 2D semi-sine shaped valleys and hills subjected to vertically propagating incident waves and ultimately introduced some simple rules to be used for the seismic design of structures found along the two-dimensional topographic structures.

** Corresponding author: kamalian@iiees.ac.ir*
[1]PhD Candidate, Department of Civil Engineering, Science and Research Branch, Islamic Azad University, Tehran, Iran
[2]Associate Professor, Department of Civil Engineering, Science and Research Branch, Islamic Azad University, Tehran, Iran
[3]Professor, Geotechnical Engineering Research Center, International Institute of Earthquake Engineering and Seismology, Tehran, Iran
[4]Assistant Professor, Schools of Geology, University College of Science, University of Tehran, Tehran, Iran

Some researchers developed the time domain boundary element formulations to model the viscoelastic behavior. Wolf and Darbre (1986) [12] used the weighted residual technique, the indirect BEM, the truncated indirect BEM and the direct BEM in time domain for 1-D dynamic problem of the spherical cavity in an infinite space. All formulations were the exact outcome, but the weighted residual technique and the truncated indirect BEM were much more appropriate than the direct BEM. Sim and Kwak (1988) [13] presented linear viscoelastic BEM in time domain by using viscoelastic fundamental solutions in terms of the constant coefficients of relaxation functions. This form required the regularity of field variables to be one order less than that of the usual formulation. Shinokawa and Mitsui (1993) [14] proposed a numerical method of viscoelastic boundary element analysis by using the time marching method and are combined with the finite element method. They applied this method to solve some numerical examples with the tunnel and excavation problems. Gaul and Schanz (1992) [15] developed a formulation for a simple viscoelastic model by using the Laplace transformed fundamental solution which is inverted within each time step. Later, Schanz (1999) [16] presented a viscoelastic formulation based on the so-called "convolution quadrature method" proposed by Lubich [17]. In this formulation, the convolution integral was numerically approximated by a quadrature formula whose weights are determined by the Laplace transform of the fundamental solution and a linear multistep method. However, inverse Laplace transformation needed to be implemented numerically in each time step, which involves high computational effort. In Feng et al. (2001) [18], a new material damping model which was convenient for use in the time domain boundary element method (TDBEM) was presented and implemented in a proposed procedure. Since only fundamental solutions for linear elastic material are employed, the procedure enjoys high efficiency and is easy to be integrated into TDBEM code. Recently, Ashrafi and Farid (2010) [19] applied a weighted residual procedure and Kelvin's fundamental solution of isotropic elastostatics to analyze viscoelastic problems with any time-dependence load and boundary conditions performance. This approach avoided the use of relaxation functions and mathematical transformations.

Regarding 2D site response analysis of topographic structures by considering material damping, to the best knowledge of the authors, only a few works have been done by the BEM, which were done in frequency domains. Semblat et al. (2000) [20] presented a boundary element method for visco-elasticity, with a Zener model. They used this method to evaluate seismic wave amplification in Nice (France) and compared the results with those of other experiments. Alvarez-Rubioa et al.(2004) [21] presented the adaptation of the formulation of DBEM, for computing 2D site effects due to the diffraction of in-plane waves at irregular sub and superficial laterally varying layered visco-elastic media. This method worked directly on frequency-domain. Tarinejad et al. (2007) [22] investigated topography effects of canyon sites using a 3D boundary element procedure in frequency domain. They used a multi-domain boundary element method proposed by Ahmad and Banerjee [23]. In additional, they investigated the effects of different wave parameters, material properties (damping ratio and poisson's ratio) and canyon geometry on site response.

Review of the literature shows that all studies on seismic behavior of viscoelastic topographic structure by using BEM were restricted to frequency domain. The important limitation of the analysis in frequency-domain is its shortcoming in non-linear problems. On the other hand, the published works on seismic behavior of topographic structure by using time domain BEM were limited to elastic case. As, the ideal model of a linear elastic soil is not adapted in dynamic analysis, it is necessary to take into account the soil damping ratio and so to use a formulation for dynamic viscoelasticity.

This paper presents a time-domain viscoelastic BEM formulation for seismic response analysis of topographic structures. Full space, two-dimensional visco-elastodynamic time-convoluted kernels are presented in order to incorporate proportional damping. The presented boundary element algorithm and derived time-convoluted kernels are applied to carry out site response analysis of viscoelastic topographic structures subjected to SV and P incident waves. The applicability and efficiency of this implemented viscoelastic BE algorithm has been demonstrated by analyzing site responses of various topographic features subjected to incident SV and P waves, including horizontally layered site, semi-circular canyon, semi-elliptical hill, slope topography and ridge section. Also, the effects of different material damping ratios on site response are investigated in time and frequency domains.

2. Governing Equation

The governing equation for an elastic, isotropic, and homogeneous body with a small amplitude displacement field can be written as:

$$\left(c_1^2 - c_2^2\right)\cdot u_{j,ij} + c_2^2 \cdot u_{i,jj} + b_i - \ddot{u}_i = 0 \tag{1}$$

in which u_i denotes the displacement vector, b_i denotes the body force vector and c_1 and c_2 are the propagation velocities of the compressional and shear waves, respectively, which are given by $C_1^2 = (\lambda + 2\mu)/\rho$; $C_2^2 = \mu/\rho$, with λ and μ being the Lame constants and ρ the mass density. The corresponding governing boundary integral equation for an elastic, isotropic, homogeneous body can be obtained using the well known weighted residual method [24] which is as follows:

$$c_{ij}(s).u_i(s,t) = \int_\Gamma \left(G_{ij}^*(x,s,t) * t_i(x,t) - F_{ij}^*(x,s,t) * u_i(x,t)\right)\cdot d\Gamma \tag{2}$$

In which, G_{ij} and F_{ij} are the transient displacement and traction fundamental solutions, respectively, and represent the displacements and tractions at a point x at time t due to a unit point force applied at s and the preceding time $t=\tau$. The terms $G_{ij} * t_i$ and $F_{ij} * u_i$ are the Riemann convolution integrals, t_i represents the traction and c_{ij} denotes the well-known discontinuity term resulting from the singularity of the F_{ij} fundamental solutions. In Equation (2), the contributions due to initial conditions and body forces are neglected. In the case of seismic loading, assuming that the total displacement can be splitted into incident ($u_j^{inc.}$) and scattered ($u_j^{sc.}$) components, the above-mentioned governing boundary integral equation should be modified as follows [25, 26]:

$$c_{ij}(s).u_i(s,t) = \int_\Gamma \left(G_{ij}^*(x,s,t) * t_i(x,t) - F_{ij}^*(x,s,t) * u_i(x,t)\right).d\Gamma + u_j^{inc.}(s,t) \tag{3}$$

Integrating by parts and considering zero initial conditions lead to the following alternative form of boundary integral equation [27]:

$$c_{ij}(s).u_i(s,t) = \int_\Gamma \left(\begin{matrix} G_{ij}^*(x,s,t) * p_i(x,t) - Z_{ij}^*(x,s,t) * u_i(x,t) \\ + W_{ij}^*(x,s,t) * v_i(x,t) \end{matrix}\right) d\Gamma + u_j^{inc.}(s,t) \tag{4}$$

In which, v_i is the velocity vector and G_{ij}^*, Z_{ij}^* *and* W_{ij}^* denote the corresponding solutions for displacement, traction and velocity respectively. The above mentioned expressions can be illustrated as follows:

$$G_{ij}^*(x,s,t-\tau) = \frac{1}{2\pi\rho}\left\{\begin{matrix} \dfrac{H(c_1t'-r)}{c_1}\left[\dfrac{2\left(\dfrac{c_1t'}{r}\right)^2-1}{\sqrt{\left(\dfrac{c_1t'}{r}\right)^2-1}}\left(\dfrac{r_{,i}r_{,j}}{r}\right)-\dfrac{\delta_{ij}}{r}\sqrt{\left(\dfrac{c_1t'}{r}\right)^2-1}\right] \\ + \dfrac{H(c_2t'-r)}{c_2}\left[-\dfrac{2\left(\dfrac{c_2t'}{r}\right)^2-1}{\sqrt{\left(\dfrac{c_2t'}{r}\right)^2-1}}\left(\dfrac{r_{,i}r_{,j}}{r}\right)+\dfrac{\delta_{ij}}{r}\dfrac{\left(\dfrac{c_2t'}{r}\right)^2}{\sqrt{\left(\dfrac{c_2t'}{r}\right)^2-1}}\right] \end{matrix}\right\} \tag{5}$$

$$W_{ij}^*(x,s,t-\tau) = \frac{c_2^2}{2\pi r c_1^2}.\frac{1}{A_1}[2r_{,i}r_{,j}\frac{\partial r}{\partial n}+\frac{\lambda}{\mu}r_{,i}.n_j] + \frac{1}{2\pi r}.\frac{1}{A_1}[\frac{\partial r}{\partial n}(\delta_{ij}-2r_{,i}r_{,j})+r_{,j}.n_i] \tag{6}$$

$$Z_{ij}^*(x,s,t-\tau) = \frac{c_2^2}{2\pi c_1 r^2}\left\{\begin{matrix} \dfrac{\partial r}{\partial n}\left[\delta_{ij}.\left(\dfrac{2}{A_1}+4A_1\right)-2r_{,i}r_{,j}\left(\dfrac{c_1(t-\tau)}{rA_1^3}-\dfrac{1}{A_1^3}+\dfrac{4}{A_1}-8A_1\right)\right. \\ \left. + n_{,i}r_{,j}\left(\dfrac{2}{A_1}+4A_1\right)+n_jr_{,i}\left(-\dfrac{\lambda}{\mu}\dfrac{c_1(t-\tau)}{rA_1^3}+\dfrac{\lambda}{\mu}\dfrac{1}{A_1^3}+\dfrac{2}{A_1}+4A_1\right)\right. \end{matrix}\right\} + \frac{c_2}{2\pi r^2}\left\{\begin{matrix} \dfrac{\partial r}{\partial n}\left[-\delta_{ij}\left(\dfrac{2}{A_2}+4A_2+\dfrac{c_2(t-\tau)}{rA_2^3}-\dfrac{1}{A_2^3}\right)+2r_{,i}r_{,j}\left(\dfrac{c_2(t-\tau)}{rA_2^3}-\dfrac{1}{A_2^3}+\dfrac{4}{A_2}+8A_2\right)\right]\right. \\ \left. - n_{,i}r_{,j}\left(\dfrac{2}{A_2}+4A_2+\dfrac{c_2(t-\tau)}{rA_2^3}-\dfrac{1}{A_2^3}\right)-n_jr_{,i}\left(\dfrac{2}{A_2}+4A_2\right)\right. \end{matrix}\right\} \tag{7}$$

Where

$$A_1 = \sqrt{\left(\frac{c_1(t-\tau)}{r}\right)^2 - 1} \tag{8}$$

$$A_2 = \sqrt{\left(\frac{c_2(t-\tau)}{r}\right)^2 - 1} \tag{9}$$

The implementation of boundary integral Equation (4) needs approximation in both temporal and spatial variations of the field variables. For temporal integration, the time axis is divided into N equal steps, so that $t = N.\Delta t$ accordingly. By using a linear time variation of the field variables, the displacement, velocity and traction are expressed as follows:

$$u_i(x,\tau) = \varphi_1(\tau)\cdot u_i^n(x) + \varphi_2(\tau)\cdot u_i^{n-1}(x) \tag{10}$$

$$\dot{u}_i(x,\tau) = \dot{\varphi}_1(\tau)\cdot u_i^n(x) + \dot{\varphi}_2(\tau)\cdot u_i^{n-1}(x) \tag{11}$$

$$p_i(x,\tau) = \varphi_1(\tau)\cdot p_i^n(x) + \varphi_2(\tau)\cdot p_i^{n-1}(x) \tag{12}$$

In which, $\varphi_1(\tau)$ and $\varphi_2(\tau)$ are linear temporal shape functions which are given by:

$$\varphi_1(\tau) = \frac{\tau - T_{n-1}}{\Delta t} \;\&\; \varphi_2(\tau) = \frac{T_n - \tau}{\Delta t} \;\&\; T_{n-1} \prec \tau \prec T_n \tag{13}$$

subscripts 1 and 2 refer to the forward and backward temporal nodes, respectively, during a time step. Thus, the time integration involves only the fundamental solutions and is expressed by:

$$G_{ij1}^{N-n+1} = \int_{(n-1)\Delta t}^{n\Delta t} G_{ij}(x,s,t-\tau)\,\varphi_1(\tau)\cdot d\tau \tag{14}$$

$$G_{ij2}^{N-n+1} = \int_{(n-1)\Delta t}^{n\Delta t} G_{ij}(x,s,t-\tau)\varphi_2(\tau) d\tau \tag{15}$$

$$F_{ij1}^{N-n+1} = \int_{(n-1)\Delta t}^{n\Delta t} \begin{pmatrix} Z_{ij}(x,s,t-\tau)\varphi_1 \\ (\tau) - W_{ij}(x,s,t-\tau)\dot{\varphi}_1(\tau) \end{pmatrix} d\tau \tag{16}$$

$$F_{ij2}^{N-n+1} = \int_{(n-1)\Delta t}^{n\Delta t} \begin{pmatrix} Z_{ij}(x,s,t-\tau)\varphi_2 \\ (\tau) - W_{ij}(x,s,t-\tau)\dot{\varphi}_2(\tau) \end{pmatrix} d\tau \tag{17}$$

After spatial discretization by using isoparametric quadratic boundary elements and some rearrangements, the convoluted BEM equation for linear temporal variation could be written as:

$$c_{ij}\cdot u_i^N(s) = \sum_{n=1}^{N}\sum_{q=1}^{Q} \left\{ \begin{array}{l} T_{ik}^n \cdot \int_{\Gamma_q} \left[G_{ij}^{N+1-n}(r)\right]\cdot \overline{N}_k(\eta)\cdot |J|\cdot d\eta - U_{ik}^n \cdot \\ \int_{\Gamma_q} \left[F_{ij}^{N+1-n}(r)\right]\cdot \overline{N}_k(\eta)\cdot |J|\cdot d\eta \end{array} \right\} + u_j^{inc.}(s,t) \tag{18}$$

where:

$$G_{ij}^{N-n+1}(r) = G_{ij1}^{N-n+1}(r) + G_{ij2}^{N-n}(r) \tag{19}$$

$$F_{ij}^{N-n+1}(r) = F_{ij1}^{N-n+1}(r) + F_{ij2}^{N-n}(r) \tag{20}$$

N denotes the last time step, Q shows the total number of boundary elements and L represents the interpolation function of an isoparametric quadratic boundary element. $G_{ij}^{N-n+1}(r)$ and $F_{ij}^{N-n+1}(r)$ are the convoluted elastodynamic displacement and traction kernels respectively, which are derived from their corresponding fundamental solutions G_{ij}, Z_{ij} and W_{ij}. The two-dimensional full space elastodynamic kernels are given as below:

$$G_{ij}^{N+1-n}(r) = \frac{1}{2\cdot\pi\cdot\rho}\cdot\sum_{k=1}^{2}\frac{1}{c_k^2}\cdot \left[\begin{array}{l} \frac{\delta_{ij}}{2}\cdot \left[\begin{array}{l} (N-n+1)\cdot\cosh^{-1}\left((N-n+1)\cdot\frac{c_k\cdot\Delta t}{r}\right) \\ -2\cdot(N-n)\cdot\cosh^{-1}\left((N-n)\cdot\frac{c_k\cdot\Delta t}{r}\right) \\ +(N-n-1)\cdot\cosh^{-1}\left((N-n-1)\cdot\frac{c_k\cdot\Delta t}{r}\right) \end{array} \right] + \\ (-1)^k\cdot\frac{1}{2}\cdot(\delta_{ij} - 2\cdot r_{,i}\cdot r_{,j})\cdot\left(\frac{c_k\cdot\Delta t}{r}\right)^2\cdot S_k - \\ (-1)^k\cdot\frac{1}{3}\cdot(\delta_{ij} - 2\cdot r_{,i}\cdot r_{,j})\cdot\left(\frac{c_k\cdot\Delta t}{r}\right)^2\cdot Q_k - \\ (-1)^k\cdot(\delta_{ij}\cdot\delta_{2k} - r_{,i}\cdot r_{,j})\cdot P_k \end{array} \right] \tag{21}$$

$$F_{ij}^{N+1-n}(r)=$$
$$\frac{\mu}{2\cdot\pi\cdot\rho\cdot r}\cdot\sum_{k=1}^{2}\left[\left\{\frac{-B_1\cdot\delta_{1k}+B_3\cdot\delta_{2k}}{c_k^2}\right\}\cdot P_k-\frac{2}{3}\cdot(-1)^k\cdot B_2\cdot\left(\frac{\Delta t}{r}\right)^2\cdot Q_k\right] \tag{22}$$

the coefficients P_k, Q_k and S_k are defined as:

$$\begin{aligned}
S_k &= (N-n+1)^2\cdot\sqrt{(N-n+1)^2-\left(\frac{r}{c_k\cdot\Delta t}\right)^2}-2\cdot(N-n)^2\cdot\sqrt{(N-n)^2-\left(\frac{r}{c_k\cdot\Delta t}\right)^2}\\
&+(N-n-1)^2\cdot\sqrt{(N-n-1)^2-\left(\frac{r}{c_k\cdot\Delta t}\right)^2}\\
P_k &= \sqrt{(N-n+1)^2-\left(\frac{r}{c_k\cdot\Delta t}\right)^2}-2\cdot\sqrt{(N-n)^2-\left(\frac{r}{c_k\cdot\Delta t}\right)^2}\\
&+\sqrt{(N-n-1)^2-\left(\frac{r}{c_k\cdot\Delta t}\right)^2}\\
Q_k &= \left\{(N-n+1)^2-\left(\frac{r}{c_k\cdot\Delta t}\right)^2\right\}^{\frac{3}{2}}-2\cdot\left\{(N-n)^2-\left(\frac{r}{c_k\cdot\Delta t}\right)^2\right\}^{\frac{3}{2}}\\
&+\left\{(N-n-1)^2-\left(\frac{r}{c_k\cdot\Delta t}\right)^2\right\}^{\frac{3}{2}}
\end{aligned} \tag{23}$$

and the coefficients B_1, B_2 and B_3 are given as:

$$\begin{aligned}
B_1 &= (\lambda/\mu).n_i.r_{,j}+2r_{,i}.r_{,j}.\frac{\partial r}{\partial n}\\
B_2 &= n_i.r_{,j}+n_j.r_{,i}+\frac{\partial r}{\partial n}.(\delta_{ij}-4.r_{,i}.r_{,j})\\
B_3 &= \frac{\partial r}{\partial n}.(2.r_{,i}.r_{,j}-\delta_{ij})-n_j.r_{,i}
\end{aligned} \tag{24}$$

By writing Equation (18) sequentially for each of the boundary nodes and transferring all known terms to the right side, the assembled system of equation takes the following matrix form:

$$F^{\mathbf{1}}\cdot U^{\mathbf{N}}=G^{\mathbf{1}}\cdot T^{\mathbf{N}}+Z^{N} \tag{25}$$

where:

$$Z^{N}=\sum_{n=1}^{N-1}\left(G^{N-n+1}\cdot T^{n}-F^{N-n+1}\cdot U^{n}\right)+U^{inc.^{N}} \tag{26}$$

U^N and T^N denote the nodal displacement and traction vectors at the current time node, respectively. Z^N includes both the effects of the past dynamic history and the incident motion on the current time node. It should be mentioned that the spatial integrals in Equations (25) and (26) could be performed easily by using the Gaussian normal quadrature rule, provided that an intelligent subsegmentation with suitable mapping is adopted to make the kernel-shape function-Jacobian product well behaved over each sub-segment. Strongly singular blocks in F^1 could be evaluated indirectly by using the concept of rigid body motion [24]. As this technique is valid only for problems with closed boundaries, the unbounded boundaries of half-plane problems should be enclosed with fictitious ones named as enclosing elements [23, 28-30].

3. Boundary Element Equation with Damping

The terms $G_{ij}^{*}*p_i$, $Z_{ij}^{*}*u_i$ and $W_{ij}^{*}*v_i$ in Equation 4 are the Riemann convolution integrals and are expressed by:

$$G_{ij}^{*}*p_i=\int_0^t u_{ij}^{*}(x,s,t-\tau)\,p_i(x,\tau)\,d\tau \tag{27}$$

$$Z_{ij}^{*}*u_i=\int_0^t z_{ij}^{*}(x,s,t-\tau)\,u_i(x,\tau)\,d\tau \tag{28}$$

$$W_{ij}^{*}*v_i=\int_0^t w_{ij}^{*}(x,s,t-\tau)\,v_i(x,\tau)\,d\tau \tag{29}$$

Assume that a unit point force is applied at a two-dimensional system at time $t=0$. If the system has a liner elastic behavior, the displacement at time t is thought to be $u_\circ(t)$. Also, if the system has viscoelastic behavior, the displacement at time t, by considering material damping equal with Equation (30). This has been carried out successfully in Ref. [18]:

$$u(t)=u_\circ(t)(1-\eta)^{(t-\tau)/2T} \tag{30}$$

In which, T is the prominent period of earthquake loading.

From a practical point of view, the coefficient of proportional damping η can be determined by other well-known models, such as viscous damping or hysteretic damping. For example, η can be related to the viscous damping ratio by Equation (31) [18]:

$$\eta = 1 - \exp(-4\pi\xi) \tag{31}$$

where, ξ is the viscous damping ratio.

Regarding to displacement relationship between the system with and without damping (Equation 30) and applying it in the integral boundary element equation, Equation 4 takes the following modified form for a viscoelastic body:

$$\begin{aligned} c_{ij}(s).u_j(s,t) = &\int_0^t \left[\int_\Gamma \left(G_{ij}^*(x,s,t-\tau).p_i(x,t) \right) d\Gamma \right] (1-\eta)^{(t-\tau)/2T} \, d\tau \\ &+ \int_0^t \left[\int_\Gamma \left(W_{ij}^*(x,s,t-\tau).v_i(x,t) \right) d\Gamma \right] (1-\eta)^{(t-\tau)/2T} \, d\tau \\ &- \int_0^t \left[\int_\Gamma \left(Z_{ij}^*(x,s,t-\tau).u_i(x,t) \right) d\Gamma \right] (1-\eta)^{(t-\tau)/2T} \, d\tau + u_{jd}^{inc.}(s,t) \end{aligned} \tag{32}$$

where $u_{jd}^{inc.}(s,t)$ is damped incident wave and $G_{ij}(x,s,t-\tau)(1-\eta)^{(t-\tau)/2T}$, $W_{ij}(x,s,t-\tau)(1-\eta)^{(t-\tau)/2T}$ and $Z_{ij}(x,s,t-\tau)(1-\eta)^{(t-\tau)/2T}$ may be defined as generalized solutions for a 2D viscoelastic problem. When the material damping is properly small, the term $(1-\eta)^{(t-\tau)/2T}$ fixed over a time increment Δt and can be put outside the boundary integration.

Then, viscoelastic boundary element equation the same as the elastic boundary element equation is presented in the previous section, but the term Z^N is modified to:

$$Z^N = \sum_{n=1}^{N-1} \left(G^{N-n+1} \cdot T^n - F^{N-n+1} \cdot U^n \right) (1-\eta)^{(N-n+1)\Delta t/2T} + U_d^{inc.N} \tag{33}$$

Comparing Equation (33) with Equation (26), the two-dimensional, full space, elastodynamic kernel G^{N-n+1} and F^{N-n+1} need to be modified to $G^{N-n+1}(1-\eta)^{(N-n+1)\Delta t/2T}$ and $F^{N-n+1}(1-\eta)^{(N-n+1)\Delta t/2T}$ for each time step, respectively. Then $G^{N-n+1}(1-\eta)^{(N-n+1)\Delta t/2T}$ and $F^{N-n+1}(1-\eta)^{(N-n+1)\Delta t/2T}$ are introduced as two-dimensional, full space, visco-elastodynamic kernels.

4. Numerical Examples

The propagation of waves in a 2D viscoelastic continuum has been calculated by the presented viscoelastic boundary element formulation. The above-mentioned formulation has been implemented in a general-purpose, vicoelastic BEM code named as VBEMSA (Viscoelastic Boundary Element Method for Seismic Analyses). The numerical examples of this section are presented to demonstrate the applicability and efficiency of the proposed time-stepping vicoelastic BE method in order to carry out site response analysis of topographical structures subjected to incident SV and P waves.

4.1. Free field motion of layered half-space

The purpose for the presentation of this example is to illustrate the applicability and accuracy of the presented vicoelastic BE algorithm, in performing one-dimensional site response analysis of a viscoelastic heterogeneous layered half-space. Fig. 1 shows a soft layer with a height of 10m and a shear wave velocity of 70.5 m/s and viscous damping ratio of 10%, overlying a stiffer half-space with a shear wave velocity of 141 m/s. The lateral boundaries of the upper bounded BEM2 zone are extended far enough in order to simulate the one-dimensional wave propagation pattern at the valley center.

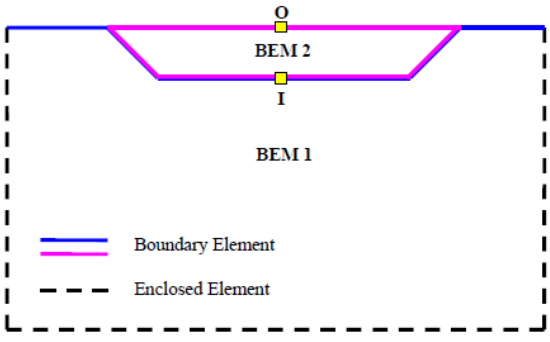

Fig. 1 Geometry and discretization of the layered half-plane problem

The mass densities and the Poisson's ratios of all materials are 2.0 ton/m^3 and 1/3, respectively. In order to discretize the problem, 145 quadratic boundary elements were used. The half-space, was also subject to vertical propagating incident SV and P waves. In all analyses, the

vertically propagating incident P and SV waves of Ricker type are adopted as a dynamic excitation. Later, Kamalian et al. [8] studied this example in elastic soil layer by using hybrid FE /BE method. The Ricker type wave equation can be presented as follows:

$$f(t) = A_{\max}\left[1 - 2(\pi f_p(t - t_0))2\right]e^{-(\pi f_p(t-t_0))^2} \quad (34)$$

f_p and t_0 denote the predominant frequency and the time shift parameter of the time history, which are chosen to be 3Hz and 0.5 s, respectively. A_{max} denotes the maximum amplitude of the time history, which is chosen as 0.0005 m. Fig. 2 shows the displacement and acceleration time histories of the incident wave.

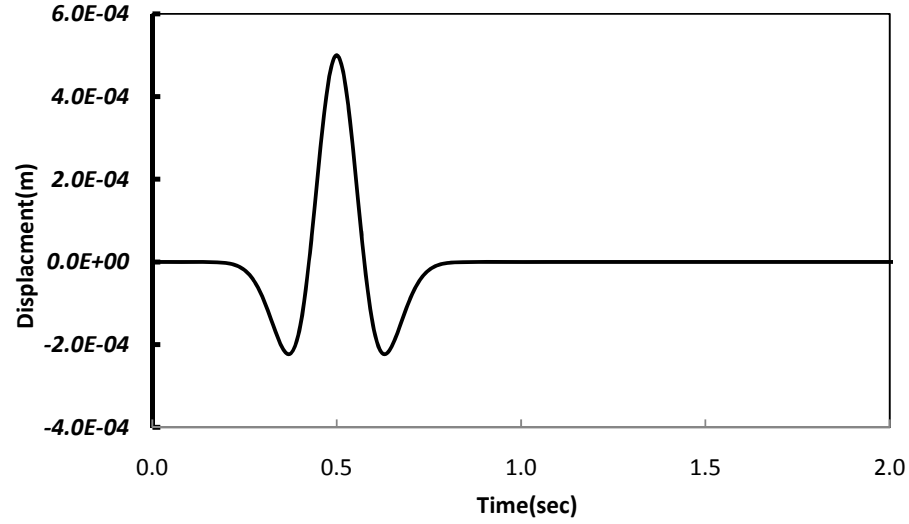

(a)

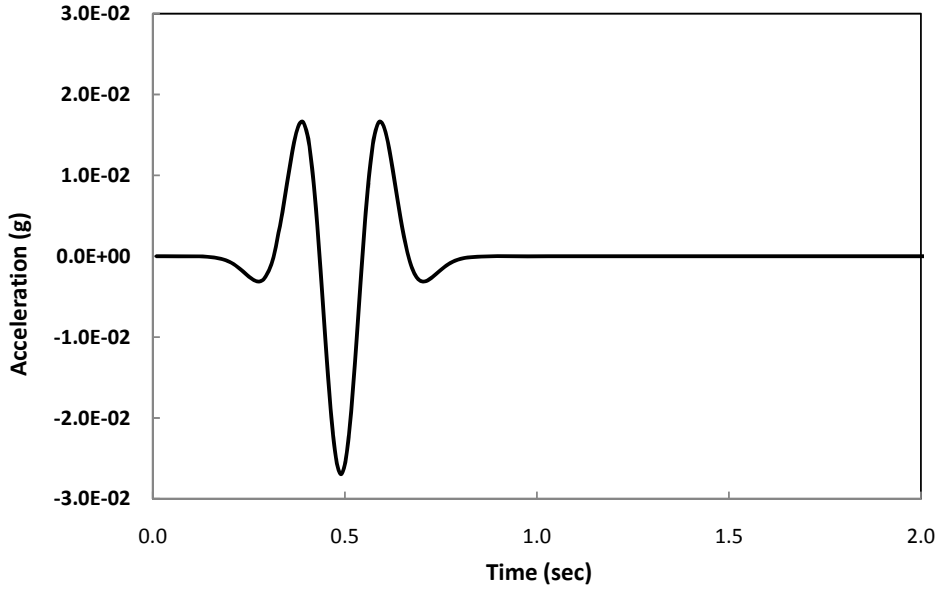

(b)

Fig. 2 (a) Displacement and (b) acceleration time histories of an incident wave

The same example is also solved with the well-known SHAKE [31] program developed specifically for one-dimensional site response analysis. The half space is defined as elastic bedrock, and the object motion is assigned to the top of the half space as with in soil layer.

Figs. 3 and 4 present the horizontal displacement time histories obtained by the VBEMSA program at top (O) and base (I) of the soft layer for different time steps, respectively. As expected, the motion at the top of the soft layer shows a delay with respect to the base, which is consistent with the difference in the shear wave velocities and also the thickness of the soft layer. Figs. 5 and 6

compare the horizontal acceleration time histories calculated by the SHAKE and VBEMSA programs at the top (O) and base (I) of the soft layer, respectively. As it can be seen, there exists an excellent agreement between the obtained results. As expected, the total vertical displacement is equal to zero. In the case of an incident P wave, there exists as well an excellent agreement between the obtained results. As expected, the total horizontal displacement is equal to zero.

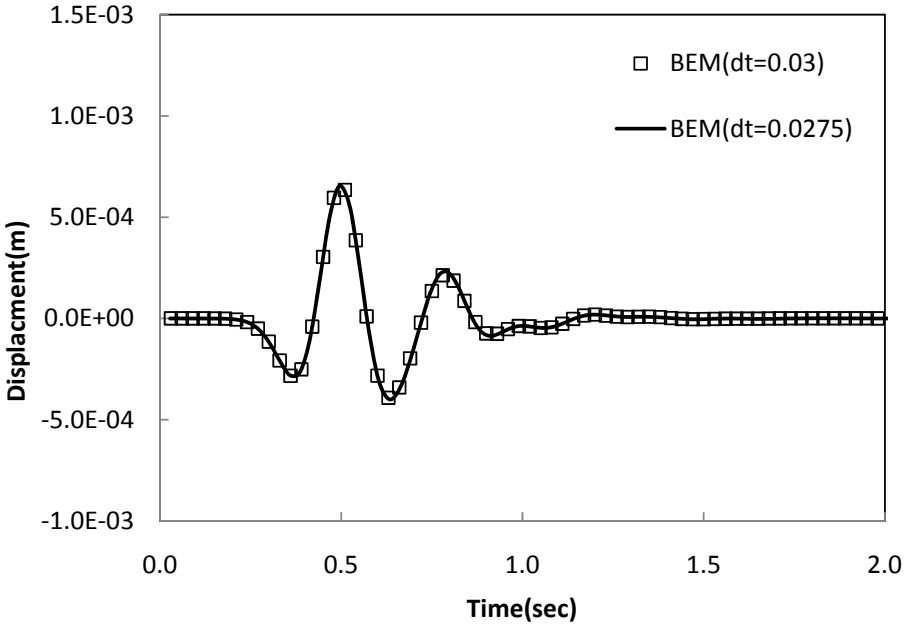

Fig. 3 Horizontal displacement time history at the base of the viscoelastic soft layer via different time steps (point I)

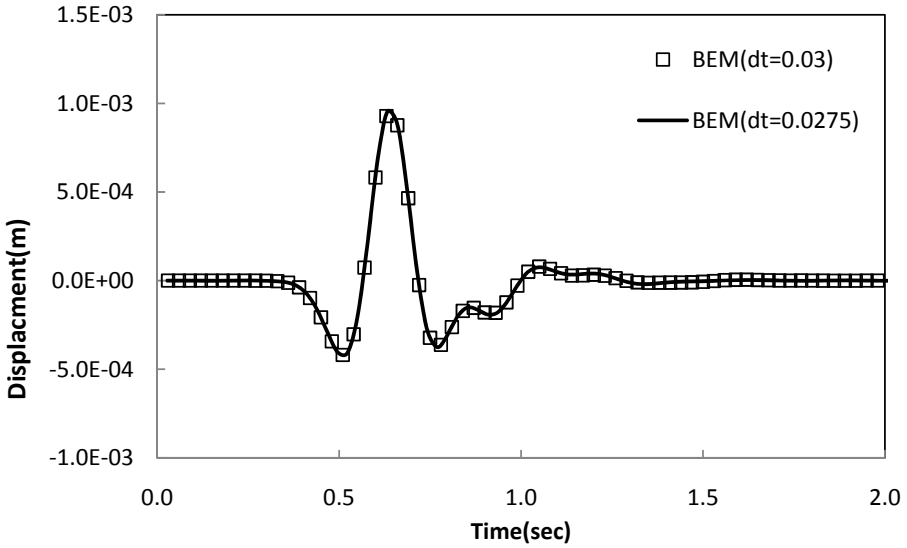

Fig. 4 Horizontal displacement time history at the top of the viscoelastic soft layer via different time steps (point O)

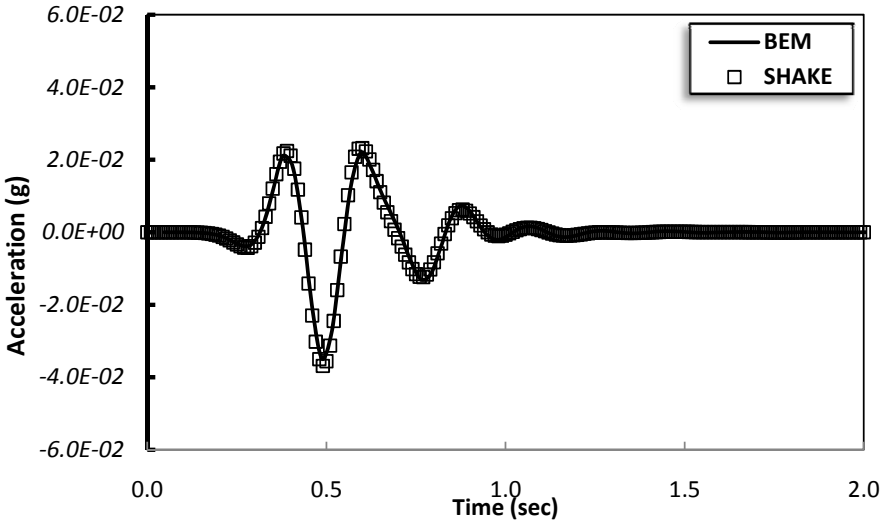

Fig. 5 Horizontal acceleration time histories at the base of the viscoelastic soft layer (point I).

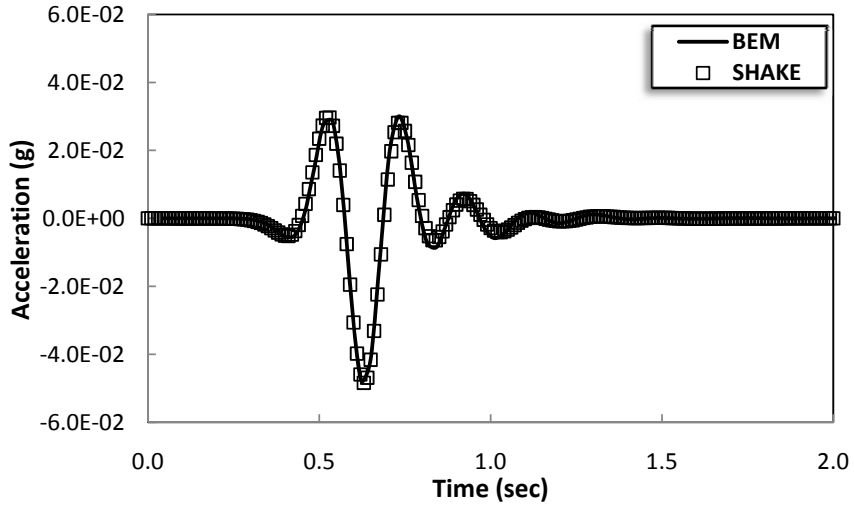

Fig. 6 Horizontal acceleration time histories at the top of the viscoelastic soft layer (point O).

Figs. 7 and 8 compare the horizontal acceleration time histories calculated by the VBEMSA programs at the top (O) and base (I) of the soft layer in the cases of elastic and viscoelastic layers, respectively. As it can be seen, the damping ratio has considerable effects on the acceleration value.

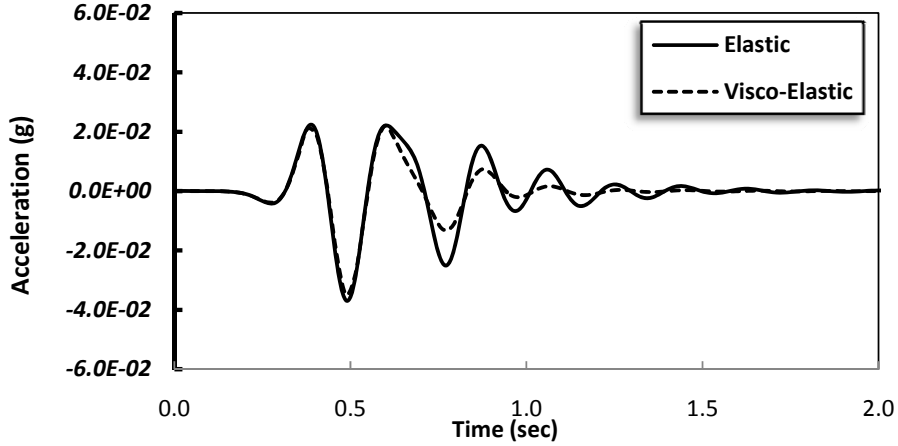

Fig. 7 Horizontal acceleration time histories at the base of the elastic and viscoelastic soft layer (point I).

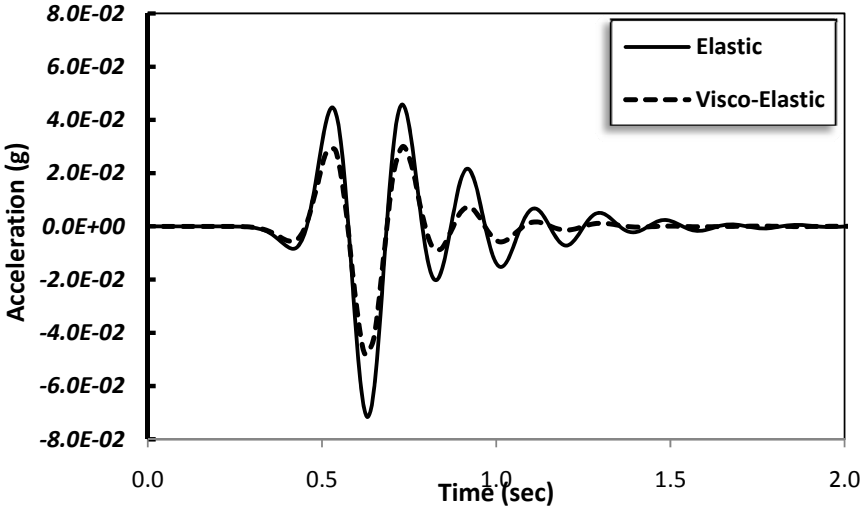

Fig. 8 Horizontal acceleration time histories at the top of the elastic and viscoelastic soft layer (point O).

4.2. Semi-circular canyon

This problem was studied in a dimensionless form by Alvarez-Rubio et al. [21] for viscoelastic media. The canyon has a radius of (r), a shear wave velocity of (c_2), a Poisson's ratio of $1/3$ and damping ratio of 1%. Fig. 9 shows the geometry and discretization of a semi-circular canyon subjected to vertically propagating incident SV and P waves of the Ricker type.

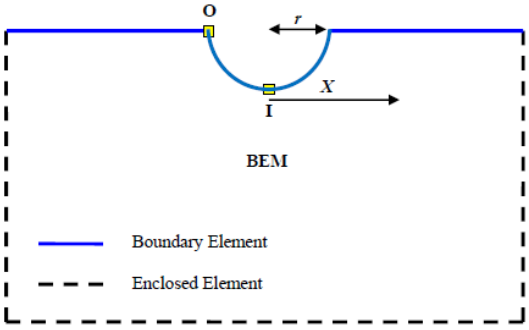

Fig. 9 Schematic geometry and discretization of a semi-circular canyon subjected to vertically propagating incident SV and P waves of the Ricker type

In order to apply the results of analyses to frequencies and geometrical conditions different from those of this study models, all results were presented in dimensionless forms. The problem was solved by using 203 quadratic boundary elements and the results are demonstrated as spectral amplifications versus dimensionless frequencies, $\Omega = \omega r / \pi c_2$ (or its inverse, the dimensionless period). In which, ω presents the angular frequency of the wave.

Figs. 10 and 11 compare the amplifications obtained by the presented VBEMSA algorithm along the canyon with those obtained by the above-mentioned work for a dimensionless frequency of 1.0 (Ω= 1.0). As can be seen, there exists excellent agreements for both vertical and horizontal components of amplification.

Fig. 12 presents the Amplification of surface displacements for a semi-circular canyon for different damping ratio in the case of an incident SV wave and Ω =1.0. Also, Fig. 13 presents the amplification of surface displacements for a semi-circular canyon for different damping ratio in the case of an incident P wave and Ω = 0.5. As it can be seen, the damping ratio has considerable effects on the amplification and de-amplification potential. Also, the results show that damping ratio does not affect the pattern of the displacement along the canyon but in order to get accurate results of topographic phenomenon, these parameters should be evaluated precisely.

Fig. 14 compares the ground responses obtained at points I and O via different time steps in case of an incident SV wave. In general, the displacement in the canyon is decreasing with damping.

4.3. Semi-elliptical hill

This problem was studied in a dimensionless form by Alvarez-Rubio et al. [21] for viscoelastic media. A semi-elliptical hill, as shown in Fig. 15, is subjected to the vertically propagating Ricker type P wave. The Ricker wave has a predominant frequency of 2 Hz, time shift parameter of 0.8 s and maximum amplitude of 0.001 m. The hill has a radius of 200 m and height of 400m. The shear wave velocity, damping ratio, Poisson's ratio and mass density are 800 m/s, 1/4, 1% and 2.23 ton/m^3, respectively. For this case, 236 quadratic boundary elements were used.

Fig. 16 compares the amplifications obtained by the presented VBEMSA algorithm along the canyon with those obtained by the above-mentioned study for a dimensionless frequency of 1.5 (Ω=1.5). As can be seen, there exist excellent agreements for both vertical and horizontal components of amplification.

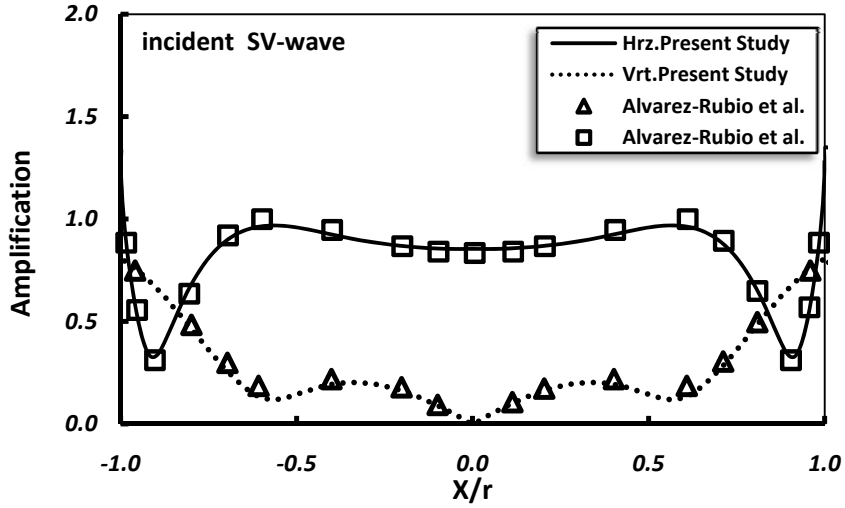

Fig. 10 Amplification of surface displacements for a semi-circular canyon in the case of an incident SV wave and Ω = 1.0. (The symbols "Hrz" and "Vrt" represent the horizontal and vertical components of amplification, respectively.)

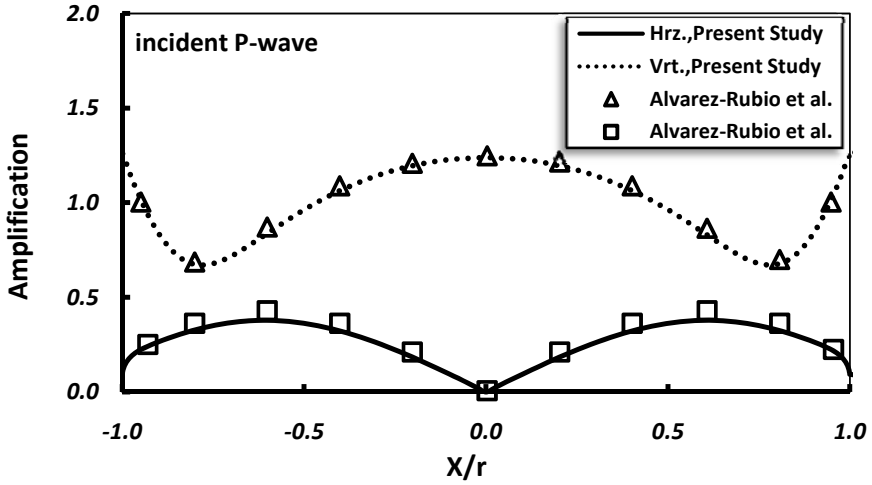

Fig. 11 Amplification of surface displacements for a semi-circular canyon in the case of an incident P wave and Ω = 1.0. (The symbols "Hrz" and "Vrt" represent the horizontal and vertical components of amplification, respectively.)

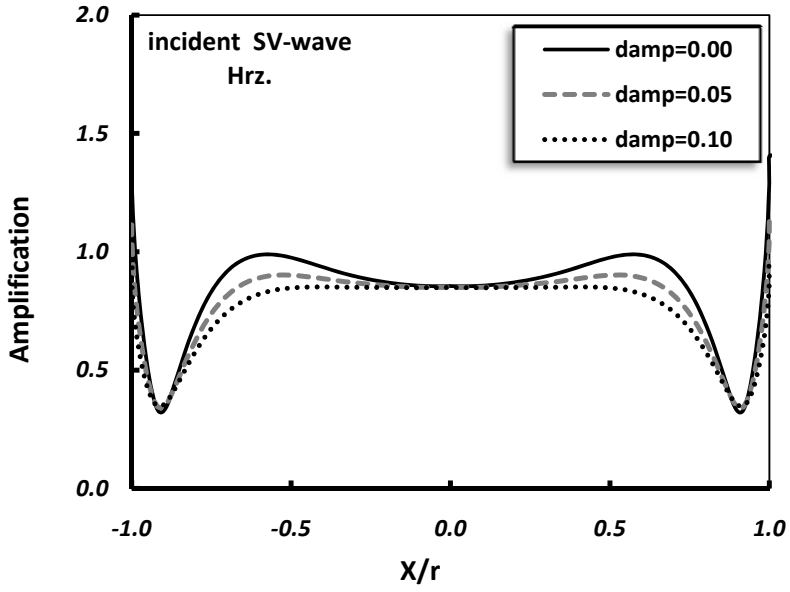

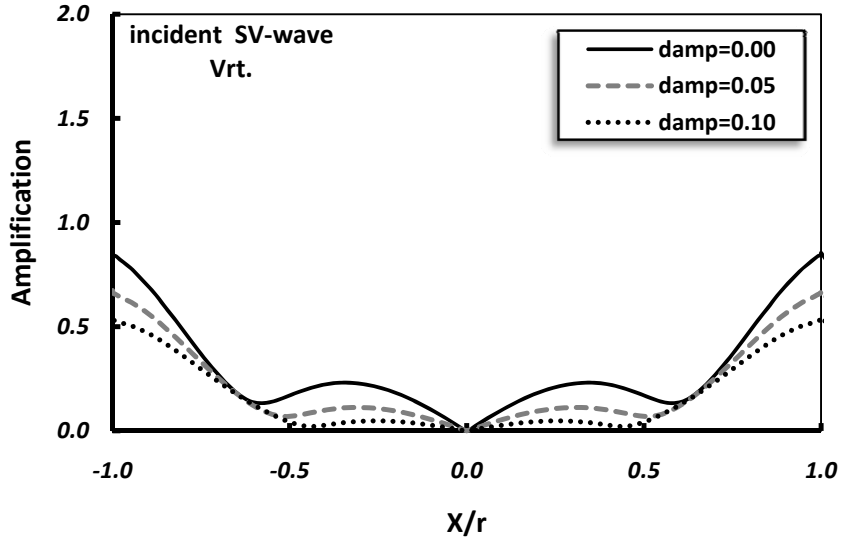

Fig. 12 Amplification of surface displacements for a semi-circular canyon for different damping ratio in the case of an incident SV wave and Ω = 1.0. (The symbols "Hrz" and "Vrt" represent the horizontal and vertical components of amplification, respectively.)

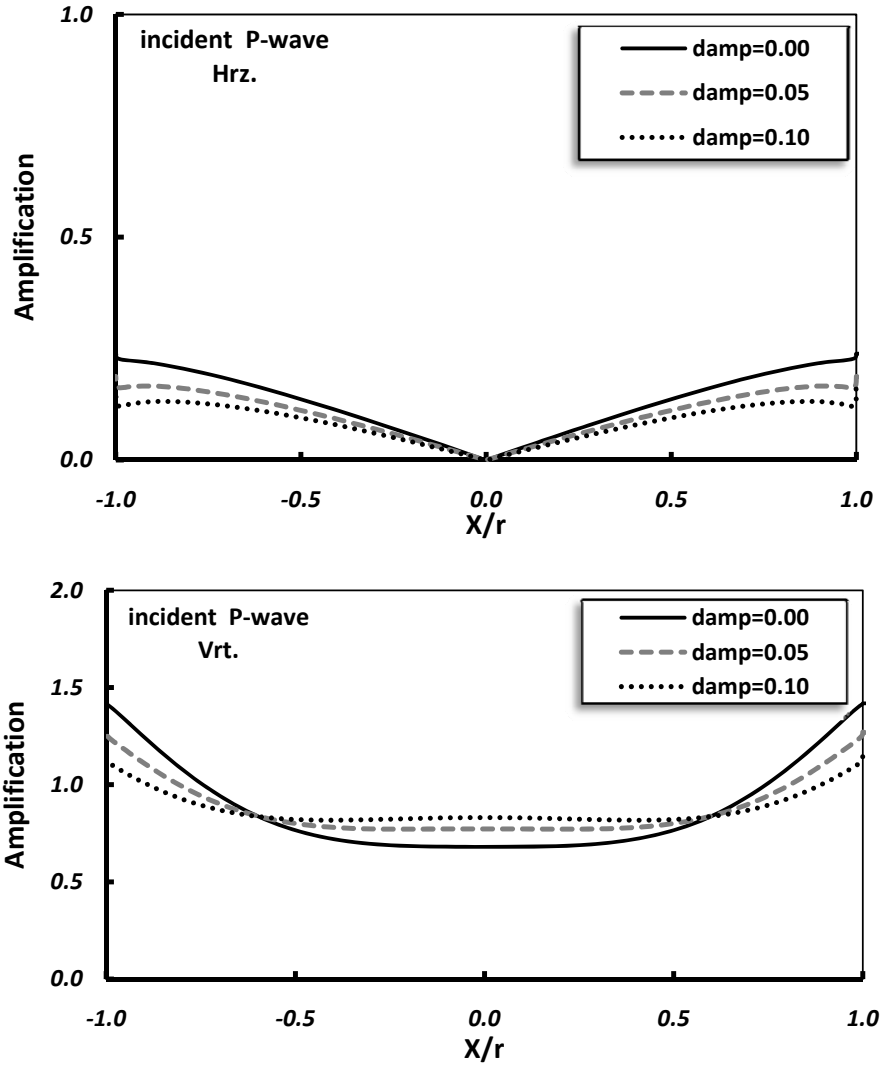

Fig. 13 Amplification of surface displacements for a semi-circular canyon for different damping ratio in the case of an incident P wave and Ω = 0.5. (The symbols "Hrz" and "Vrt" represent the horizontal and vertical components of amplification, respectively.)

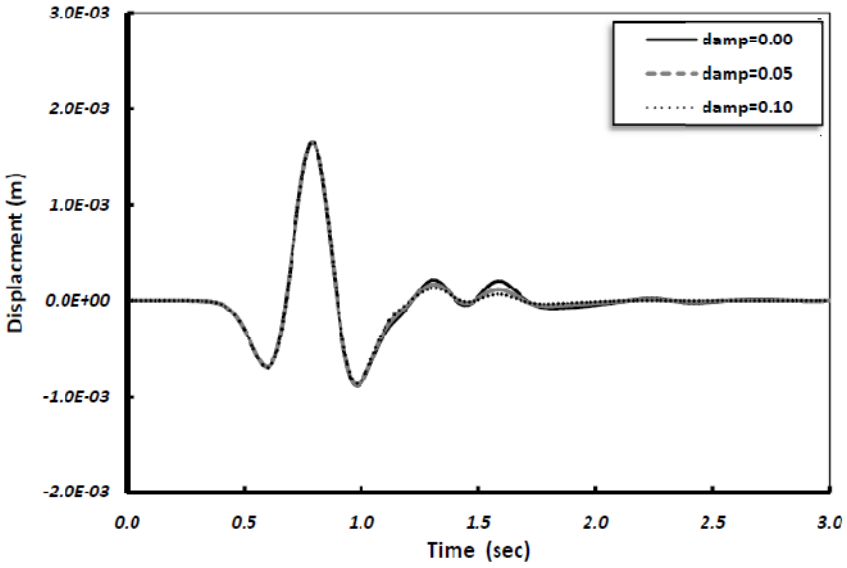

(a)

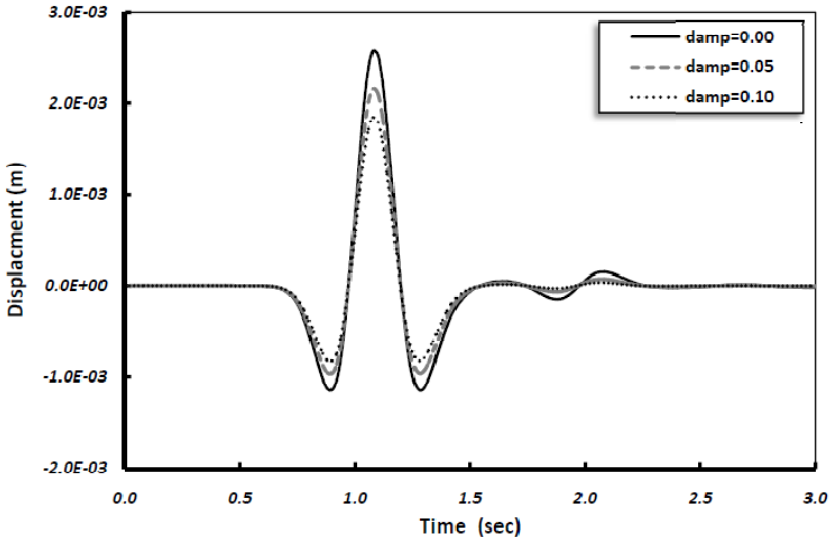

(b)

Fig. 14 Horizontal displacement time histories via different damping ratio for SV wave. (a) point I, (b) point O

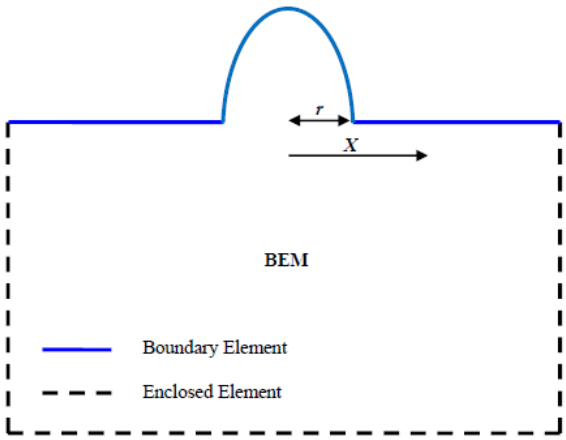

Fig. 15 Schematic geometry and discretization of a semi-elliptical hill subjected to vertically propagating incident SV and P waves of the Ricker type.

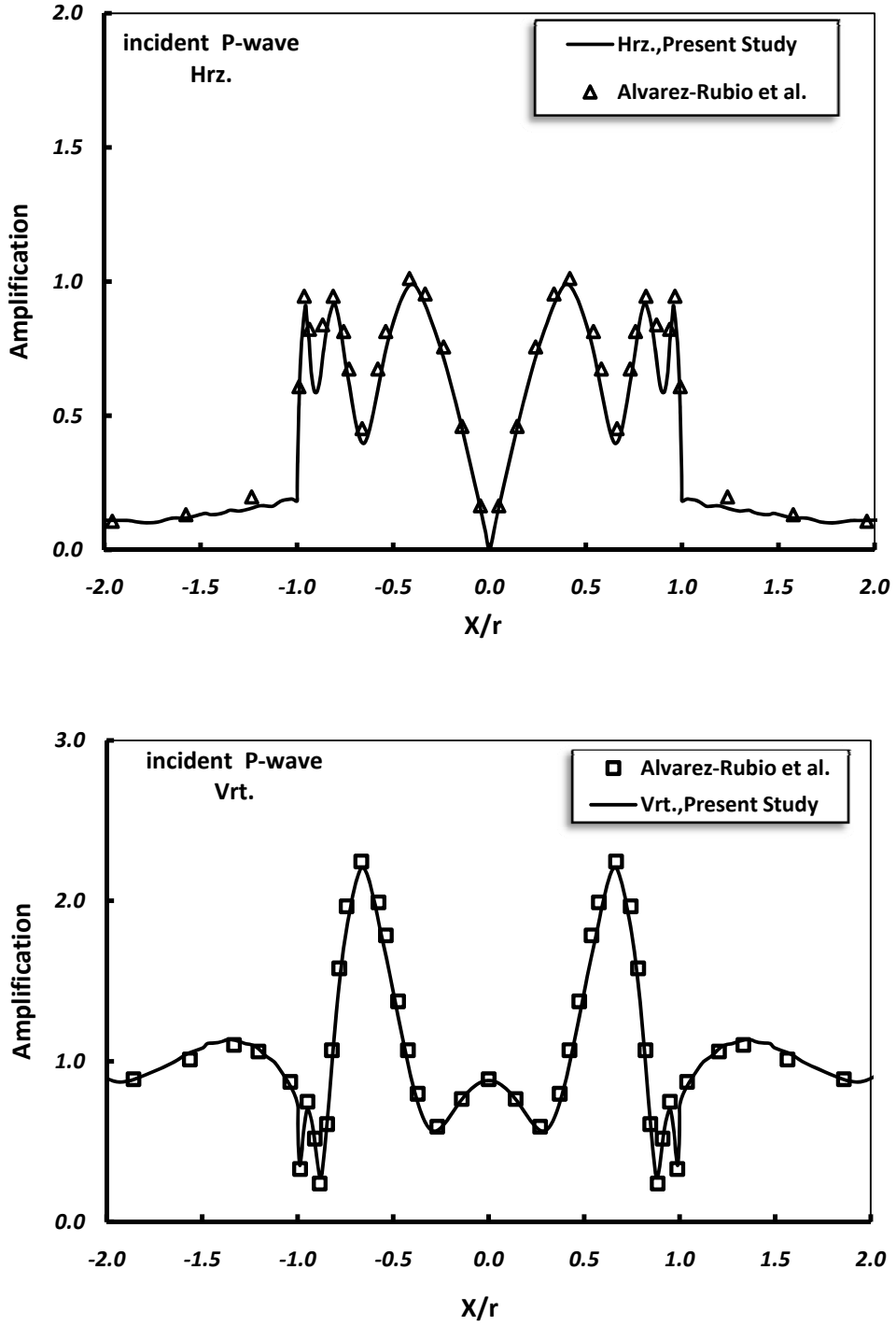

Fig. 16 Amplification of surface displacements for a semi-elliptical hill in the case of an incident P wave and Ω = 1.5. (The symbols "Hrz" and "Vrt" represent the horizontal and vertical components of amplification, respectively.)

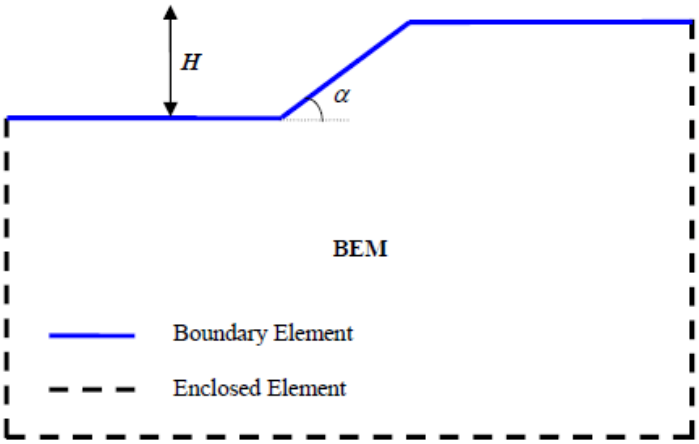

Fig. 17 Schematic geometry and discretization of a slope topography subjected to vertically propagating incident SV and P waves of the Ricker type.

4.4. Slope topography

This problem was studied in a dimensionless form by Bouckovalas and Papadimitriou [32] for viscoelastic media using computer code FLAC. Slope topography, as shown in Fig. 17, is subjected to the vertically propagating Ricker type SV wave.

The specific case of uniform soil with slope inclination $\alpha = 60^\circ$ was analyzed. The shear wave velocity, damping ratio, Poisson's ratio and mass density are 800 m/s, 1/3, 5% and 2.00 ton/m^3, respectively. The Ricker wave has a predominant frequency of 3 Hz, time shift parameter of 0.45 s and maximum amplitude of 0.001 m.

The problem was solved by using 351 quadratic boundary elements. The results are demonstrated as spectral amplifications versus dimensionless frequencies, $\Omega = fH/c_2 = H/\lambda$. In which, f and λ present the angular frequency and wavelength of the shear wave, respectively.

Fig. 18 compares our results at the crest of step-like slopes with the respective results from [32] and shows that the two distinctly different methodologies of analyses (Viscoelastic Boundary Element method here versus generalized consistent Finite Difference method in [32]) produce practically identical results.

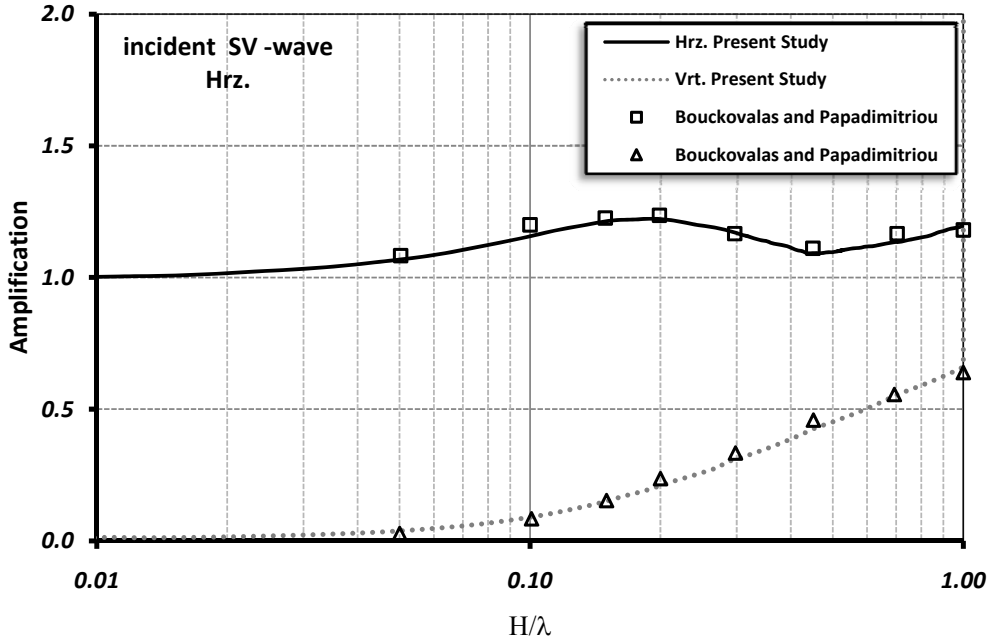

Fig. 18 The variation of crest amplification factor versus the dimensionless frequency for uniform slopes with $\alpha = 60^\circ$.

4.5. Semi-circular-shaped ridge

The purpose for the presentation of this example is to illustrate the applicability of the presented viscoelastic BE algorithm in performing site response analysis of ridge structures. A semi-circular-shaped ridge, as shown in Fig. 19, is subjected to the vertically propagating Ricker type SV and P wave. The Ricker wave has a predominant frequency of 3 Hz, time shift parameter of 0.45 s and maximum amplitude of 0.001 m. The ridge has a radius of 200 m. The shear wave velocity, Poisson's ratio and mass density are 800 m/s, 1/3 and 2.23 ton/m^3, respectively. As far as this case is concerned, 203 quadratic boundary elements were used. The amplification of horizontal and vertical components of ground motion with respect to the free field motion, for a dimensionless frequency of 1.0 in the case of an incident SV wave for different damping ratios is demonstrated in Fig. 20.

Fig. 21 presents the time-domain ground responses obtained at the top (point I in Fig. 19) and bottom (point O in Fig. 19) of the semi-circular-shaped hill in the cases of an incident SV wave for different damping ratios, respectively. For the incident SV wave, as expected, the vertical displacement is equal to zero.

Also, the amplification for horizontal and vertical components of ground motion with respect to the free field motion, for a dimensionless frequency of 0.5 in the case of an incident P wave for different damping ratios is demonstrated in Fig 22.

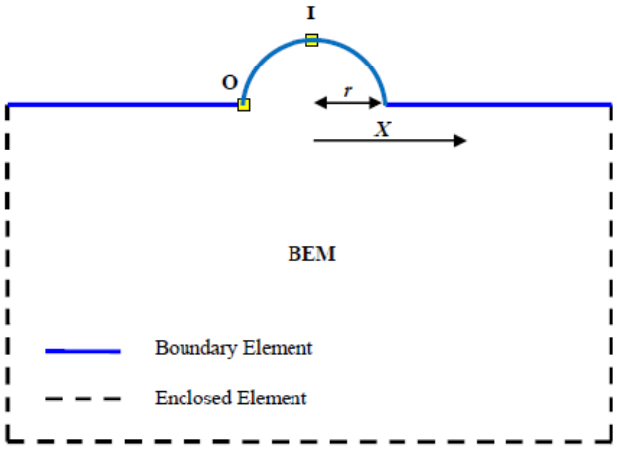

Fig. 19 Schematic geometry and discretization of a semi-circular shaped hill subjected to vertically propagating incident SV and P waves of the Ricker type.

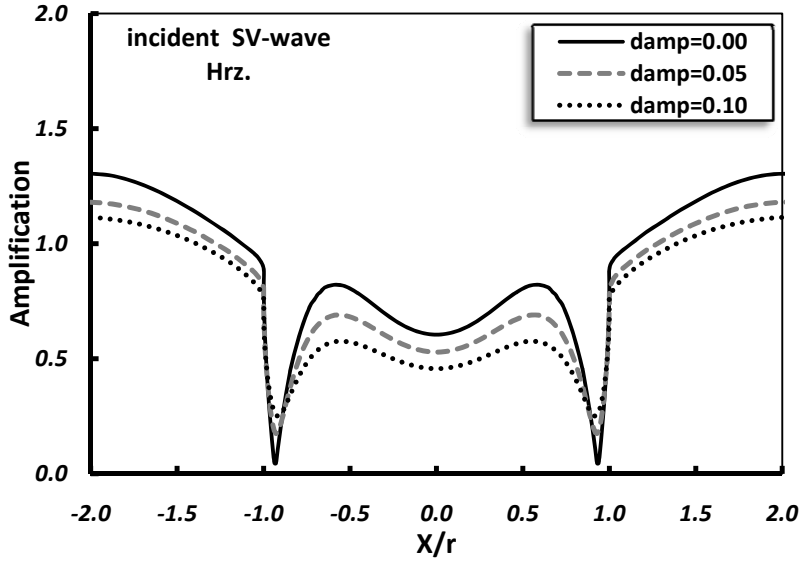

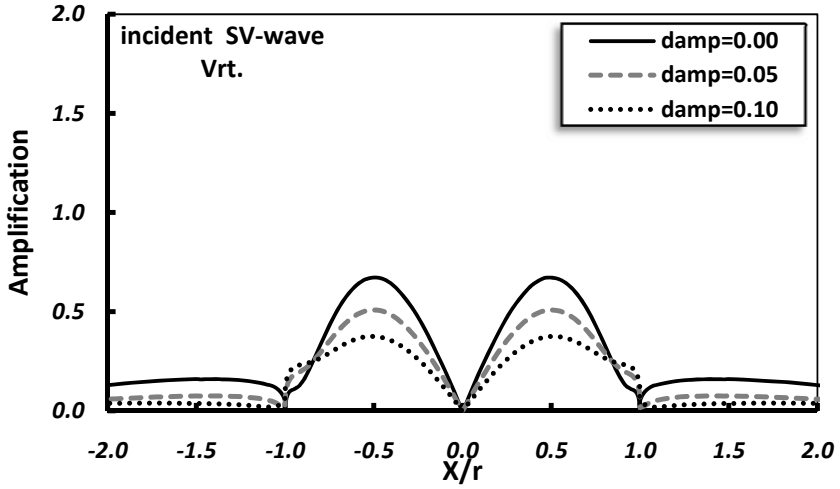

Fig. 20 Amplification of surface displacements for a semi-circular shaped hill for different damping ratio in the case of an incident SV wave and Ω = 1.0. (The symbols "Hrz" and "Vrt" represent the horizontal and vertical components of amplification, respectively.)

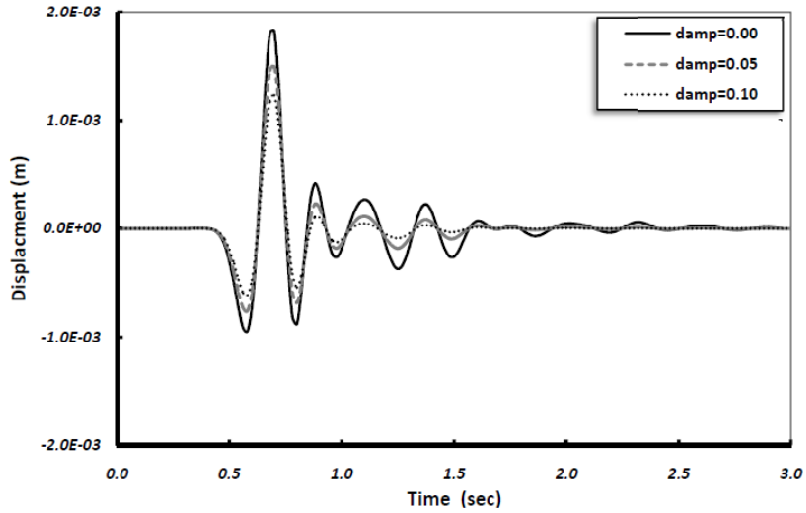

(a)

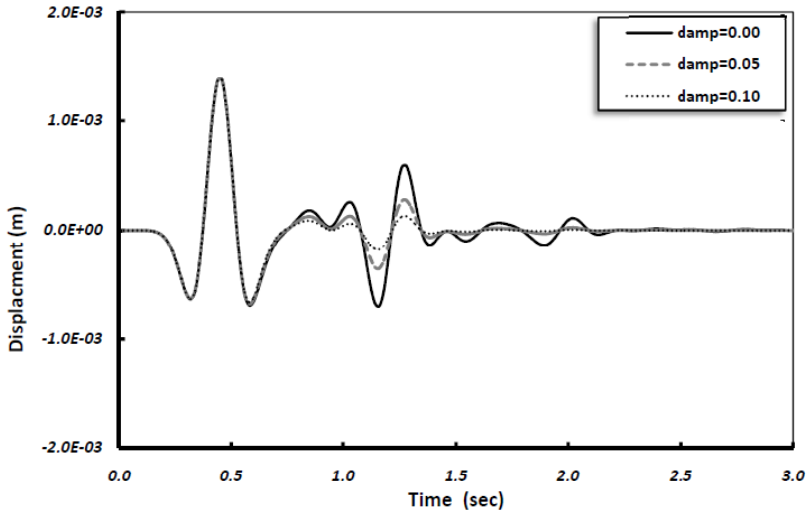

(b)

Fig. 21 Horizontal displacement time histories via different damping ratio for a semi-circular shaped hill in the case of SV wave. (a) point *I*, (b) point *O*

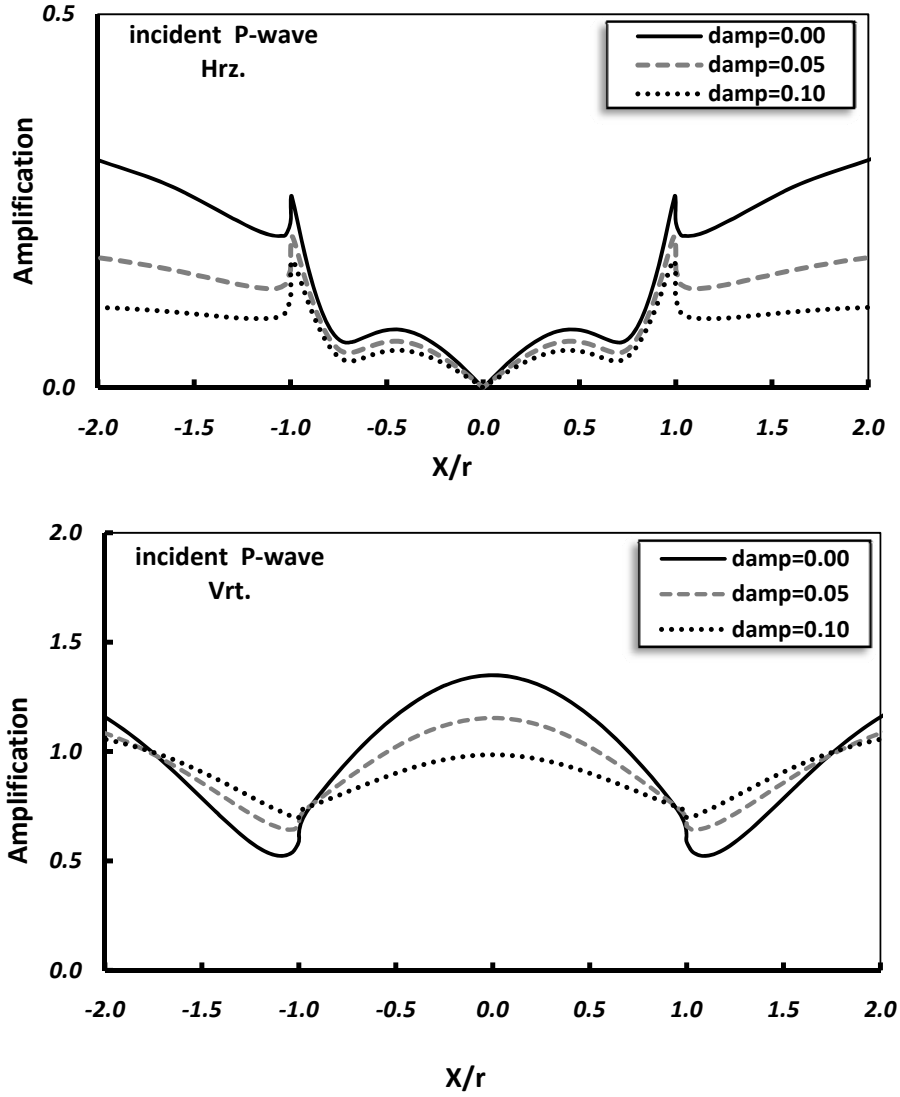

Fig. 22 Amplification of surface displacements for a semi-circular shaped hill for different damping ratio in the case of an incident P wave and Ω = 0.5. (The symbols "Hrz" and "Vrt" represent the horizontal and vertical components of amplification, respectively.)

5. Conclusion

In this paper the advanced time stepping BEM for transient two-dimensional site response analysis of topographic structures is extended to viscoelastic areas. Full-space two-dimensional time-convoluted visco-elastodynamic kernels have been derived analytically and applied.

The accuracy of the visco-elastodynamic kernels as well as the applicability and efficiency of the viscoelastic BEM algorithm have been demonstrated through various classic examples of site response analysis including a horizontally layered site, a semi-circular canyon, a semi-elliptical hill, slope topography and ridge sections subjected to vertically propagating incident SV and P waves. Since the viscoelastic BEM algorithm is completely formulated in the time domain, it forms a basis for extending site response analysis of two-dimensional topographic structures to non-linear behavior in the future. The numerical results confirm that damping ratio does not affect the general pattern of the amplification potential of the topography but can play a key role in controlling its intensity.

References

[1] Bouchon M. Effect of topography on surface motion, Bulletin of the Seismological Society of America, 1973, Vol. 63, pp. 615–632.

[2] Antes H, Von Estorff O.V. Seismic response amplification due to topographic influences, Proceedings of the Ninth World Conference on Earthquake Engineering, Tokyo-Kyoto, Japan, 1988, Vol. III, pp. 411– 416.

[3] Takemiya H, Fujiwara A. SH-wave scattering and propagation analysis at irregular sites by time domain

BEM, Bulletin of the Seismological Society of America, 1994, Vol. 84, pp. 1443–1455.
[4] Adam M, Takemiya H. Seismic wave amplification in Kobe during Hyogo-ken Nanbu earthquake, Proceedings of the 11th World Conference on Earthquake Engineering, Paper No.1885, Acapulco, Mexico, 1996.
[5] Takemiya H, Adam M. Seismic wave amplification due to topography and geology in Kobe during Hyogo-Ken Nanbu earthquake, Structural Engineering Earthquake Engineering, 1997, Vol. 14, pp. 129-138.
[6] Takemiya H, Adam M. 2-D nonlinear seismic ground analysis by FEM-BEM: The case of Kobe in the Hyogo-Ken Nanbu earthquake, Structural Engineering Earthquake Engineering, 1998, Vol. 15, pp. 19-27.
[7] Kamalian M, Gatmiri B, Sohrabi-Bidar A. On time-domain two-dimensional site response analysis of topographic structures by BEM, Journal of Seismology and Earthquake Engineering, 2003, Vol. 5, pp. 35–45.
[8] Kamalian M, Jafari M.K, Sohrabi Bidar A, Razmkhah A, Gatmiri B. Time-domain two-dimensional site response analysis of non-homogeneous topographic structures by a hybrid FE/BE method, Soil Dynamic and Earthquake Engineering, 2006, No. 8, Vol. 26, pp. 753-765.
[9] Kamalian M, Gatmiri B, Sohrabi Bidar A, Khalaj A. Amplification pattern of 2D semi-sine-shaped valleys subjected to vertically propagating incident waves, Communication in Numerical Method in Engineering, 2007, Vol. 23, pp. 871–887.
[10] Kamalian M, Jafari M.K, Sohrabi Bidar A, Razmkhah A. Seismic response of 2d semi-sine shaped hills to vertically propagating incident waves: amplification patterns and engineering applications, Earthquake Spectra, 2008, Vol. 24, pp. 405-430.
[11] Kamalian M, Sohrabi Bidar A, Razmkhah A, Taghavi A.A, Rahmani I. Considerations on seismic microzonation in areas with two-dimensional hills, Journal of Earth System Science (JESS), 2008, No. S2, Vol. 117, pp. 783-796.
[12] Wolf J.P, Darbre G.R. Time-domain boundary element method in visco-elasticity with application to a spherical cavity, Soil Dynamics and Earthquake Engineering, 1986, Vol. 5, pp. 138 -148.
[13] Sim W.J, Kwak B.M. Linear viscoelastic analysis in time domain by boundary element method, Computers & Structures, 1988, No. 4, Vol. 29, pp. 531-539.
[14] Shinokawa T, Mitsui Y. Application of boundary element method to geotechnical analysis, Computers and Structures, 1993, No. 2, Vol. 47, pp. 179-187.
[15] Gaul L, Schanz M. BEM formulation in time domain for viscoelastic media based on analytical time integration, Proceedings of 14th Boundary Element International Conference, Sevilla, Spain, 1992, Vol. II, pp. 223-234.
[16] Schanz M, A boundaey element formolation in time domain for viscoelastic solids, Communication in Numerical Method in Engineering, 1999, Vol. 15, pp. 799-809.
[17] Lubich C. Convolution quadrature and discretized operational calculus, I Numerische Mathematik, 1988, Vol. 52, pp. 129-145.
[18] Feng J, Pekau O.A, Chuhan H.Z. A 2-D time-domain boundary element method with damping, International Journal for Numerical Method in Engineering, 2001, Vol. 51, pp. 647-661.
[19] Ashrafi H, Farid M. A general boundary element formulation for the analysis of viscoelastic problems, International Journal of Engineering, Transactions A: Basics, 2010, No. 2, Vol. 23, pp. 153-167.
[20] Semblata J.F, Duvalb A.M, Dangla P. Numerical analysis of seismic wave amplification in Nice (France) and comparisons with experiments, Soil Dynamics and Earthquake Engineering, 2000, Vol. 19, pp. 347-362.
[21] Alvarez-Rubio S, Sanchez-Sesma F.J, Benitoc J.J, Alarcon E. The direct boundary element method: 2D site effects assessment on laterally varying layered media (methodology), Soil Dynamics and Earthquake Engineering, 2004, Vol. 24, pp. 167–180.
[22] Tarinejad R, Ahmadi M.T, Khaji N. Analysis of topographic amplification effects on canyon sites using 3D boundary element method, Journal of Seismology and Earthquake Engineering, 2007, Vol. 9, pp. 25–37.
[23] Ahmad S, Banerjee P.K. Multi-domain BEM for two-dimensional problems of elastodynamics, International Journal for Numerical Methods in Engineering, 1988, Vol. 26, pp. 891–911.
[24] Brebbia C.A, Dominguez J. Boundary elements, an Introductory Course, Computational Mechanics Publications, Southampton, Boston, 1989.
[25] Kawase H. Time-domain response of a semi-circular canyon for incident P, SV and Rayleigh waves calculated by the discrete wave number boundary element method, Bulletin of the Seismological Society of America, 1988, Vol. 78, pp. 1415–1437.
[26] Hadely P.K, Askar A, Cakmak A.S. Scattering of waves by inclusions in a nonhomogeneous elastic half space solved by boundary element methods, Technical Report NCEER-89-0027, 1989.
[27] Dominguez J. Boundary elements in dynamics, Computational Mechanics Publications, Elsevier Applied Science, Amsterdam, 1993.
[28] Israil A.S.M, Banerjee P.K. Advanced time domain formulation of BEM for two-dimensional transient elastodynamics, International Journal for Numerical Methods in Engineering, 1990, Vol. 29, pp. 1421–1440.
[29] Israil A.S.M, Banerjee P.K. Two-dimensional transient wave propagation by time domain BEM, International Journal of Solids and Structures, 1990, Vol. 26, pp. 851–864.
[30] Israil A.S.M, Banerjee P.K. Advanced development of boundary element method for two-dimensional dynamic elasto-plasticity, International Journal of Solids and Structures, 1992, Vol. 29, pp. 1433–1451.
[31] Schnabel P.B, Lysmer J, Seed H.B. SHAKE-A computer program for earthquake response analysis of horizontally layered sites, Report no EERC-72-12, Berkeley, CA: Earthquake Engineering Research Center, 1972.
[32] Bouckovalas G.D, Papadimitriou A.G. Numerical evaluation of slope topography effects on seismic ground motion, Soil Dynamics and Earthquake Engineering, 2005, Vol. 25, pp. 547–558.